ACS APPLIED MATERIALS & INTERFACES

www.acsami.org

Research Article

Overcoming Aggregation-Induced Quenching by Metal–Organic Framework for Electrochemiluminescence (ECL) Enhancement: Zn-PTC as a New ECL Emitter for Ultrasensitive MicroRNAs Detection

Jun-Mao Wang, Li-Ying Yao, Wei Huang, Yang Yang, Wen-Bin Liang, Ruo Yuan, and Dong-Rong Xiao*

Cite This: *ACS Appl. Mater. Interfaces* 2021, 13, 44079–44085

Read Online

ACCESS | Metrics & More | Article Recommendations | Supporting Information

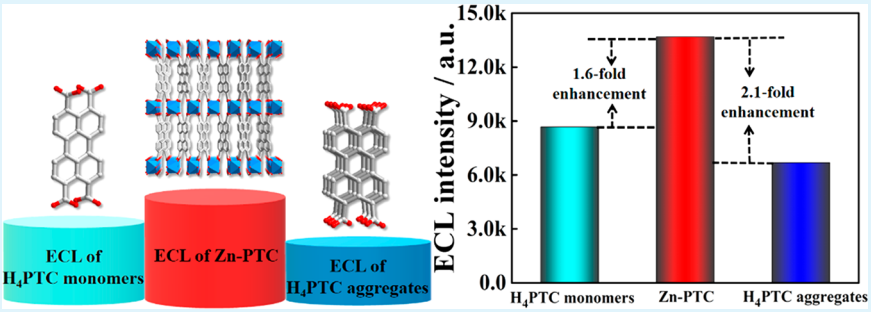

ABSTRACT: Polycyclic aromatic hydrocarbons (PAHs) as traditional electrochemiluminescence (ECL) luminophores have been widely applied in the analysis field. However, their ECL intensity and efficiency are still limited due to the aggregation-induced quenching (ACQ) effect of PAHs. Hence, to overcome this limitation, we put forward a new strategy to increase the ECL intensity and efficiency by eliminating the ACQ effect of PAHs through the coordinative immobilization of PAHs within metal–organic frameworks (MOFs). As anticipated, the proof-of-concept experiment indicated that the coordinative immobilization of perylene-3,4,9,10-tetracarboxylate (PTC) into a Zn-PTC MOF could distinctly increase the ECL intensity and efficiency compared with H_4PTC aggregates and H_4PTC monomers. The reason for the ECL enhancement of Zn-PTC was that the immobilization of PTC within the MOF effectively amplified the distance between perylene rings of PTC ligands and thus eliminated the ACQ effect. Furthermore, the PTC into Zn-PTC was stacked in an edge-to-edge mode to form J-aggregation, which was also conducive to ECL enhancement. On the basis of the excellent ECL performance, we utilized Zn-PTC as a new ECL emitter combined with exonuclease III-stimulated target cycling and DNAzyme-assisted cycling dual amplification strategies to construct an ECL sensor for microRNA-21 detection, which had a wide signal response (100 aM to 100 pM) with a detection limit of 29.5 aM. Overall, this work represents a new and convenient method to overcome the ACQ effect of PAHs and boost the ECL performance, which opens a new horizon for developing high-performance ECL materials, thus offering more opportunities for building highly sensitive ECL biosensors.

KEYWORDS: *metal–organic frameworks, polycyclic aromatic hydrocarbons, aggregation-induced quenching effect, biosensor, microRNA-21*

1. INTRODUCTION

MicroRNAs (miRNAs) are a kind of diminutive and endogenous single-stranded RNA, which are associated with numerous cancers.[1,2] Among them, miRNA-21 is considered to be a vital cancer marker because it is overexpressed in dozens of different types of tumor cells.[3] At present, numerous analytical methods including electrochemical,[4] fluorescence,[5] Raman,[6] and electrochemiluminescence (ECL)[7] have been extensively used in the detection of miRNAs. In comparison with other detection methods mentioned above, the ECL technique is particularly attractive due to its high sensitivity, low background, and rapid response.[8,9] However, because the concentrations of miRNAs in early stage cancers are extremely low,[10] it is very urgent to construct an ultrasensitive ECL sensor for miRNAs detection at the early stage of cancers.

One general method for improving the sensitivity of ECL sensors involves the construction of high-performance ECL materials to obtain strong ECL emission. The ECL materials can be classified into three major categories, i.e., inorganic

Received: July 11, 2021
Accepted: August 26, 2021
Published: September 13, 2021

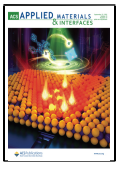

https://doi.org/10.1021/acsami.1c13086
ACS Appl. Mater. Interfaces 2021, 13, 44079–44085

Scheme 1. (A) Preparation of Zn-PTC. (B) Exo III-Stimulated Target Cycling Process. (C) Fabrication of the Proposed Biosensor

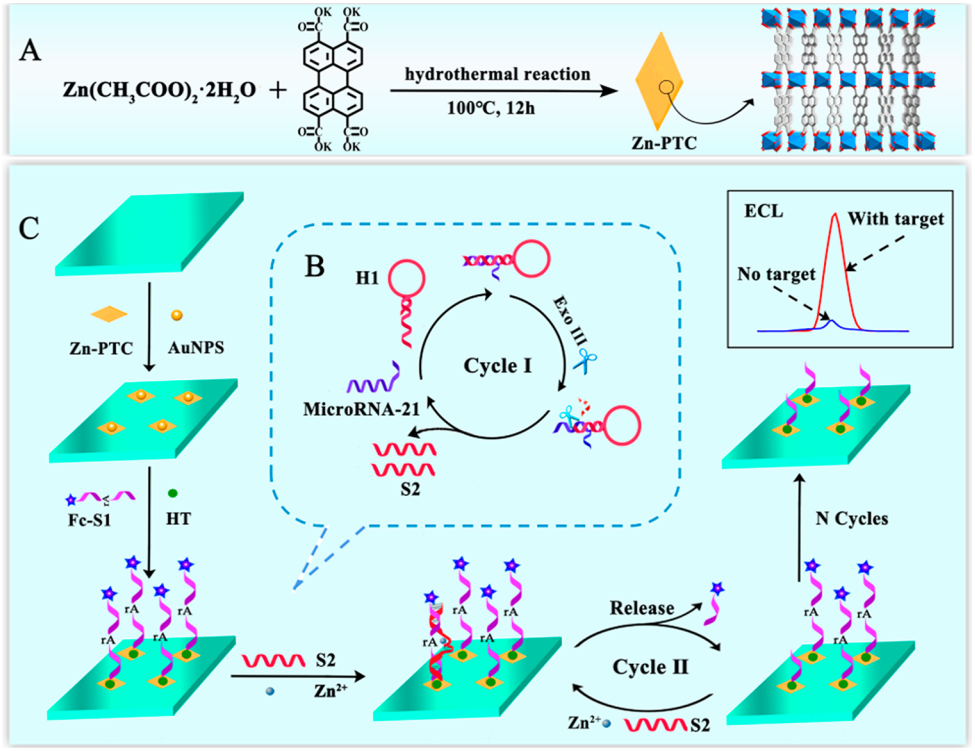

emitters, organic emitters, and nanomaterials.[11] Among them, organic emitters have attracted much attention owing to their unique advantages including structural diversity and tailorability, tunable luminescent properties, good biocompatibility, and low cost.[12] Polycyclic aromatic hydrocarbons (PAHs) with large planar π-conjugation belong to conventional organic emitters, which have a prominent position in the ECL field because of their high quantum yield, excellent photoelectron properties, and superior chemical stability.[13,14] Unfortunately, in the aggregate state, most PAHs and their derivatives suffer from aggregation-induced quenching (ACQ). Tang et al. also pointed out that the PAH molecules tended to aggregate in face-to-face stacking (H-aggregation), due to strong $\pi-\pi$ interactions between the aromatic rings, resulting in decreased luminescence efficiency.[15] To overcome the problem of ACQ, Tang and co-workers successfully turned ACQ luminophores into aggregation-induced emission (AIE) luminogens by decorating the ACQ cores (e.g., perylene bisimide, pyrene, anthracene, etc.) with AIE molecules, which disrupted the molecular planarity and suppressed $\pi-\pi$ stacking due to their twisted structures.[16−22] These works indicated that the suppression of $\pi-\pi$ stacking between aromatic rings was an effective way to surmount the ACQ effect of PAHs. Nevertheless, almost all reported examples relied on covalent bonds to connect the ACQ luminophores to AIE molecules, which presented some disadvantages such as complex synthesis, more byproducts, and difficult separation. Hence, searching for a convenient strategy to eradicate the ACQ effect of PAHs is highly imperative. Inspired by the context mentioned above, herein we proposed a new and easy-to-perform strategy to enhance the ECL efficiency and intensity by overcoming the ACQ issue of PAHs through the coordinative immobilization of PAHs within metal−organic frameworks (MOFs). Such a strategy can enlarge the distance between π-planes of PAHs and suppress $\pi-\pi$ stacking, thus eradicating the ACQ effect.

As an emerging class of porous materials, MOFs have received tremendous attention in ECL sensing fields because their well-ordered porosity and high surface area can greatly enhance the loading amount of ECL luminophores.[23−29] Nowadays, for most reported MOF-based ECL materials, $Ru(bpy)_3^{2+}$ and its derivatives, as the most commonly employed luminophores, are immobilized into MOFs by doping, encapsulation, or postmodification.[30−34] However, $Ru(bpy)_3^{2+}$ and its derivatives are expensive and possess potential biotoxicity, which impede their large-scale application. Besides, because of their bulky steric hindrance, Ru-complexes are difficult to immobilize into the inner cavities of MOFs, thus imposing restrictions on the loading number of luminophores. Therefore, it is of great significance to develop a new strategy and screen appropriate luminophores for synthesizing Ru-complex-free MOF-based ECL materials with low cost, good biocompatibility, high loading amount of luminophores, and outstanding ECL performance.

Bearing the above-mentioned points in mind, we conducted a proof-of-concept experiment to synthesize Zn-PTC MOF by selecting the inexpensive and readily available perylene-3,4,9,10-tetracarboxylate (PTC) as the organic ligand. As expected, the ECL intensity of Zn-PTC was superior to those of H_4PTC aggregates and H_4PTC monomers, which can be attributed to the following reasons. First, when PTC ligands were immobilized in Zn-PTC, the distance between PTC ligands was increased, thereby reducing detrimental $\pi-\pi$ stacking interactions and greatly weakening the ACQ effect to improve the ECL intensity and efficiency. Second, PTC ligands within Zn-PTC were no longer assembled to form H-aggregation but stacked in an edge-to-edge mode to form J-aggregation. In contrast to H-aggregates with weak emission, J-

https://doi.org/10.1021/acsami.1c13086
ACS Appl. Mater. Interfaces 2021, 13, 44079−44085

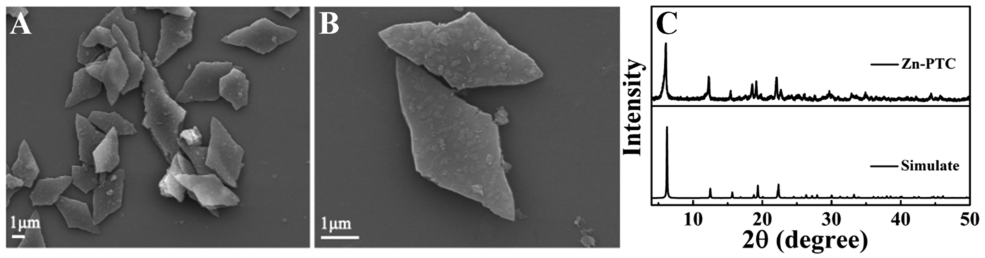

Figure 1. (A, B) SEM images of Zn-PTC. (C) XRPD pattern and simulated pattern of Zn-PTC.

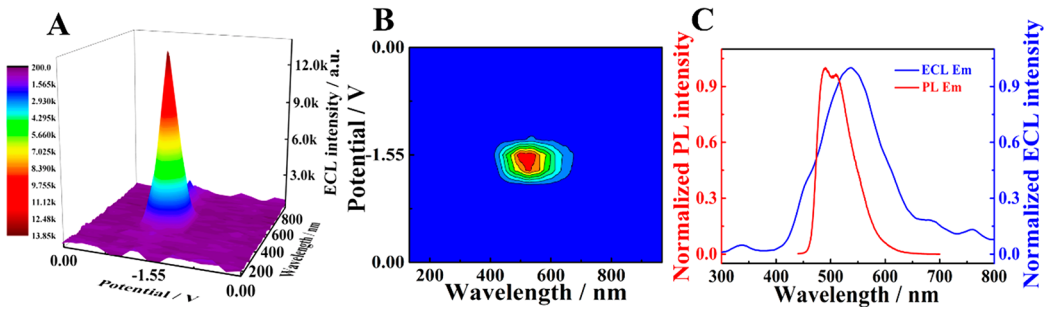

Figure 2. (A) ECL−potential−wavelength 3D surface map and (B) 2D heat map image of Zn-PTC/GCE in PBS with $S_2O_8^{2-}$. (C) Normalized ECL emission spectrum and PL emission spectrum of Zn-PTC.

aggregates exhibit high solid-state luminescence efficiency and thus benefit the enhancement of ECL emission.[35−37] Finally, the PTC luminophores were directly employed as organic ligands to synthesize MOFs, which immensely increased the loading content of the ECL luminophores.

In view of the aforesaid excellent ECL performance of Zn-PTC, herein an "off−on" ECL biosensor was fabricated for ultrasensitive miRNA-21 analysis by employing Zn-PTC as a high-performance ECL indicator combined with exonuclease III (Exo III)-stimulated target cycling and Zn^{2+}-dependent DNAzyme-assisted cycling dual amplification strategies. Initially, as illustrated in Scheme 1A, Zn-PTC was prepared by self-assembly of PTC and $Zn(CH_3COO)_2{\cdot}2H_2O$. The Exo III-stimulated target cycling amplification process is depicted in Scheme 1B. The hairpin DNA (H1) could recognize and hybridize with target miRNA-21 to form an H1−miRNA-21 complex, which was subsequently cleaved by Exo III to release miRNA-21 for recycling (cycle I) and to generate the simulated target (output S2, a Zn^{2+}-dependent DNAzyme). Meanwhile, as depicted in Scheme 1C, Zn-PTC was decorated onto the surface of the working electrode to obtain strong ECL emission. Then Au nanoparticles (AuNPs) were dropped onto the above modified electrode to further assemble the thiol and ferrocene (Fc)-labeled ssDNA with the DNAzyme cleavage site (Fc-S1), which quenched the ECL signal of Zn-PTC and thus gained a "signal off" state. Afterward, the output S2 was introduced to the surface of the modified electrode and hybridized with Fc-S1. With the aid of cofactor Zn^{2+}, Fc-S1 was cleaved by DNAzyme, leading to the liberation of the Fc-labeled DNA segment from the electrode surface. When the vast majority of Fc-labeled DNA segments were removed, a recovered ECL signal was acquired ("signal on" state). Satisfactorily, the proposed ECL sensor accomplished the ultrasensitive determination of miRNA-21 with a detection limit of 29.5 aM. Meaningfully, overcoming the ACQ effect of PAHs by coordinatively immobilizing PAHs within MOFs for ECL enhancement provides a new strategy to synthesize high-efficiency ECL emitters, thereby creating a new method to construct ultrasensitive ECL sensors.

2. EXPERIMENTAL SECTION

2.1. Fabrication of the Biosensor. Initially, the glassy carbon electrode (GCE) was preprocessed in accordance with the previously reported method.[38] Then 10 μL of Zn-PTC dispersion (1 mg/mL) was dropped onto the electrode surface to get a homogeneous film. Subsequently, 5 μL of AuNPs dispersion was coated on the modified electrode and dried at room temperature. Next, 10 μL of Fc-S1 (2.0 μM) was incubated on the AuNPs/Zn-PTC/GCE surface at 4 °C overnight. After rinsing with PBS, Fc-S1/AuNPs/Zn-PTC/GCE was incubated with hexanethiol (HT) solution (10 μL, 1 mM) for 60 min to block the nonspecific binding sites. Finally, a 10 μL mixture of S2 and Zn^{2+} solution (the preparation of S2 DNA is described in Supporting Information) was dropped onto the decorated electrode surface and incubated at 37 °C for 90 min.

2.2. ECL Measurement Procedure. After construction of the biosensor, the ECL measurement was conducted in 2 mL of PBS solution (pH 7.4, 0.1M) containing 2.5 mM $S_2O_8^{2-}$ with a scanning scope of −1.55 to 0 V (scan rate: 300 mV/s).

3. RESULTS AND DISCUSSION

3.1. Characterization of Zn-PTC. The morphologies of Zn-PTC were characterized by scanning electron microscopy (SEM). As observed in Figure 1A and 1B, Zn-PTC possesses rhombus lamella shapes. In addition, as shown in Figure S1, compared with the perylene-3,4,9,10-tetracarboxylic dianhydride (PTCDA) precursor, the characteristic bands of C═O and C−O−C stretching vibrations disappeared in the FT-IR spectrum of Zn-PTC. Furthermore, the stretching vibrations of COO^- (1545 and 1359 cm^{-1}) were observed, which proved the coordination between the carboxylate groups of PTC and Zn^{2+}. Moreover, as exhibited in Figure 1C, the crystal structure of Zn-PTC was determined by X-ray powder diffraction (XRPD). The XRPD pattern of Zn-PTC matched well with the simulated XRPD pattern, indicating that Zn-PTC with high phase purity was successfully synthesized. The structure of Zn-PTC exhibited an interesting 3D open framework, which was

https://doi.org/10.1021/acsami.1c13086
ACS Appl. Mater. Interfaces 2021, 13, 44079−44085

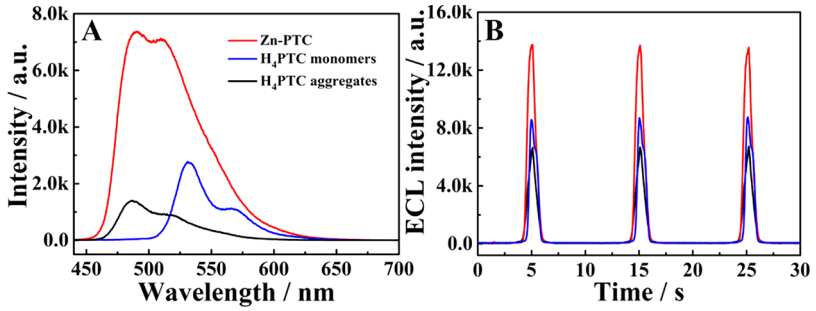

Figure 3. (A) Fluorescence spectra of 10^{-5} M H_4PTC in PBS (black curve), 10^{-5} M H_4PTC in DMF (blue curve), and Zn-PTC containing 10^{-5} M PTC in PBS (red curve). (B) ECL−time profiles of GCE in PBS with 1 mM H_4PTC (black curve), in 0.35 M $TBAPF_6$ DMF with 1 mM H_4PTC (blue curve), and in PBS with Zn-PTC including 1 mM PTC (red curve).

constructed from 1D Zn−O−Zn chains cross-linked by PTC ligands (Figure S2A and S2B). As depicted in Figure S2C, the PTC ligands were arranged in a slipped fashion. The minimum distance between the perylene rings of adjacent PTC ligands was 3.627 Å and the slip angle (θ) was 29.07° (Figure S2C), which is in perfect accordance with the characteristic parameters of J-aggregation.[35]

3.2. Luminescence Properties of Zn-PTC. The luminescence properties of Zn-PTC were evaluated by ECL and photoluminescence (PL) spectral analyses. As demonstrated in Figure 2A, the ECL−potential−wavelength 3D color image of Zn-PTC was investigated to observe the evolution process of ECL emission under a scan potential of −1.55 to 0 V. Meanwhile, both the 2D heat map image (Figure 2B) and the ECL emission spectrum (Figure 2C) of Zn-PTC clearly showed that the strongest ECL peak was located at 536 nm. Moreover, the maximum PL emission peak of Zn-PTC was at 490 nm upon photoexcitation at 430 nm (Figure 2C). Apparently, the ECL emission of Zn-PTC was red-shifted 46 nm compared to PL, which might be attributed to the self-absorption of Zn-PTC and/or instrument effects in ECL spectral test.[39,40]

3.3. PL and ECL Enhancement of Zn-PTC. To prove the correctness of the proposed luminescence enhancement strategy, the PL and ECL intensities of H_4PTC aggregates, H_4PTC monomers, and Zn-PTC were compared under identical conditions. As expected, the PL intensity of H_4PTC monomers in DMF (Figure 3A) was obviously enhanced compared with that of H_4PTC aggregates dispersed in water, attesting that the ACQ effect really existed in H_4PTC aggregates. More interestingly, the PL intensity of Zn-PTC was approximately 2.7, 5.3-fold higher than those of H_4PTC monomers and H_4PTC aggregates (Figure 3A), which preliminarily proved the validity of our proposed strategy that the coordinative immobilization of PAHs within MOFs can eliminate the ACQ effect of PAHs to achieve luminescence enhancement.

Meanwhile, a similar trend was also revealed in the comparison of ECL intensities of H_4PTC aggregates, H_4PTC monomers, and Zn-PTC. As shown in Figure 3B, the ECL intensity of Zn-PTC was about 1.6 times and 2.1 times those of H_4PTC monomers and H_4PTC aggregates. Moreover, when the $[Ru(bpy)_3]^{2+}$ system was taken as a reference (5%), the relative ECL efficiency (Φ_{ECL}) of the Zn-PTC/$S_2O_8^{2-}$ system was calculated as 15.98%, which was significantly higher than those of H_4PTC monomers/$S_2O_8^{2-}$ (Φ_{ECL} = 9.19%) and H_4PTC aggregates/$S_2O_8^{2-}$ (Φ_{ECL} = 7.83%) systems (the details are shown in Supporting Information section S12). The ECL enhancement of Zn-PTC could be attributed to the following reasons. (1) PTC as bridging ligands were fixed into Zn-PTC MOF, which enlarged the distance between perylene rings of PTC ligands, thus overcoming the ACQ effect to realize ECL enhancement. (2) The PTC ligands within Zn-PTC were arranged in a slipped fashion to form J-aggregation (Figure S2). Different from H-aggregates with low or no luminescence, J-aggregates commonly showed high solid-state luminescence efficiency, which was conducive to ECL enhancement. Therefore, it is a promising and effective strategy to increase the ECL intensity and efficiency by surmounting the ACQ effect of PAHs through the coordinative immobilization of PAHs within MOFs.

3.4. Possible ECL Mechanism of the Zn-PTC/$S_2O_8^{2-}$ System.

$$S_2O_8^{2-} + e^- \rightarrow SO_4^{2-} + SO_4^{\cdot-} \quad (1)$$

$$\text{Zn-PTC} + e^- \rightarrow \text{Zn} - \text{PTC}^{\cdot-} \quad (2)$$

$$\text{Zn-PTC}^{\cdot-} + SO_4^{\cdot-} \rightarrow \text{Zn-PTC}^* + SO_4^{2-} \quad (3)$$

$$\text{Zn-PTC}^* \rightarrow \text{Zn-PTC} + \hbar\nu \quad (4)$$

3.5. Analytical Performance of the ECL Biosensor. The analytical performance of the biosensor was evaluated by quantitative determination of miRNA-21 under optimum conditions (Supporting Information section S14). As depicted in Figure 4A, the ECL intensity strengthened gradually with

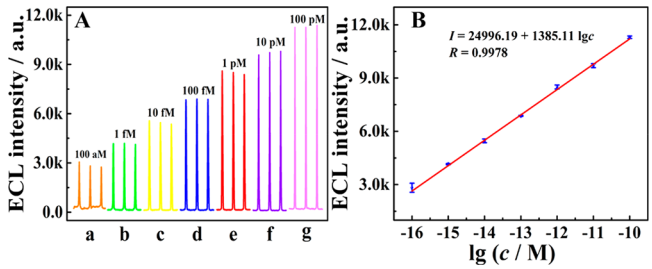

Figure 4. (A) ECL responses toward different miRNA-21 concentrations. (B) Linear correlation plot for miRNA-21 detection.

the incremental concentration of miRNA-21 from 100 aM to 100 pM. Furthermore, the ECL intensity exhibited an admirable linear relationship with the logarithmic value of miRNA-21 concentrations (Figure 4B). The linear equation was I = 1385.11 lg c + 24996.19 (R = 0.9978), and the detection limit was calculated as 29.5 aM based on the standard 3σ rule.[41] Additionally, in a comparison of miRNA-21

https://doi.org/10.1021/acsami.1c13086
ACS Appl. Mater. Interfaces 2021, 13, 44079−44085

detection with some previously reported bioassays (Table 1), it was found that our biosensor owned a lower detection limit.

Table 1. Comparison of Different Works for miRNA-21 Detection

detection methods	linear range	detection limit	ref
EC	2 fM to 1 nM	2 fM	42
flourescence	0−500 fM	3 fM	43
ECL	5 fM to 500 pM	1.51 fM	44
ECL	0.5 fM to 10 pM	0.24 fM	45
ECL	100 aM to 100 pM	29.5 aM	this work

According to these results, we could conclude that the designed biosensor possessed a preeminent analytical performance for precise detection of miRNA-21.

3.6. Selectivity, Stability, and Reproducibility of the ECL Biosensor. Selectivity, stability, and reproducibility were of great significance for the practicability of biosensor. So, to assess the selectivity of this biosensor, five different miRNAs (miRNA-144, miRNA-155, miRNA-429, miRNA-141, and miRNA-199a) and thrombin binding aptamer (TBA) were selected as interferences. As displayed in Figure 5A, the ECL responses of the above-mentioned interfering miRNAs (10 nM) had little change compared with that of blank sample. Meanwhile, the ECL responses showed barely negligible changes between the mixture (10 nM interfering miRNAs and 100 pM miRNA-21) and pure miRNA-21 (100 pM). These results proved that the proposed biosensor could selectively recognize miRNA-21. In addition, the stability of this biosensor was appraised upon scanning for 18 cycles (100 fM miRNA-21) consecutively. As presented in Figure 5B, the biosensor displayed stable ECL signals and the relative standard deviation (RSD) was 1.48%, proving the satisfactory stability of this biosensor. Simultaneously, the reproducibility was appraised by intra-assays (the same electrode tested five times) and interassay (each of the five electrodes was measured once) experiments at 1 pM miRNA-21, and the RSDs were only 0.91% and 0.69%, respectively, illustrating that this ECL sensor has acceptable reproducibility (Figure 5C).

3.7. Application. To evaluate the practicability of the as-prepared biosensor, we chose the lysates of cervical cancer cells (Hela) and human breast cancer cells (MCF-7) for detection. From Figure 6, the ECL emission was markedly enhanced with the increment of MCF-7 cell numbers, demonstrating that target miRNA-21 was greatly expressed in MCF-7 cells. Conversely, the ECL intensity increased slowly with the increase in Hela cell numbers, which suggested that miRNA-21 expression was low in the Hela cells. These experimental results were compatible with recent reports,[46] revealing that this proposed biosensor could be applied for monitoring miRNA-21 expression in cancer cells.

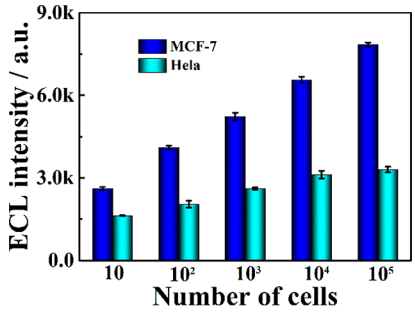

Figure 6. ECL analysis of the proposed biosensor in MCF-7 and Hela cells.

4. CONCLUSION

In summary, we have proposed a new and convenient strategy to enhance ECL by eliminating the ACQ effect of PAHs via coordinative immobilization of PAHs within MOFs. As expected, the ECL intensity and efficiency of Zn-PTC MOF prepared according to this strategy were much higher than those of H_4PTC aggregates and H_4PTC monomers, not only because the coordinative immobilization of PTC within Zn-PTC efficiently enlarged the distance between perylene rings of PTC ligands, which surmount the ACQ effect and improve the ECL emission, but also because the PTC ligands within Zn-PTC stacked in an edge-to-edge mode to form J-aggregation, which further enhances the ECL intensity and efficiency. Considering the excellent ECL performance of Zn-PTC, it was employed as an ECL beacon to construct a novel ECL biosensor, which realized the highly selective and sensitive detection of miRNA-21. In short, this proof-of-concept work provides a simple and efficient method to eliminate the ACQ effect for ECL enhancement, which improves the prospects for exploiting high-performance ECL emitters, thereby revealing a new path to construct ultrasensitive ECL sensors.

■ ASSOCIATED CONTENT

Supporting Information

The Supporting Information is available free of charge at https://pubs.acs.org/doi/10.1021/acsami.1c13086.

Reagents and materials, apparatus, synthesis of AuNPs, preparation of S2 DNA oligonucleotides, synthesis, structure, and stability of Zn-PTC, measurement procedure for ECL, the measurement of ECL emission spectrum for Zn-PTC, the FT-IR spectra for Zn-PTC and PTCDA, electrochemical study of Zn-PTC and

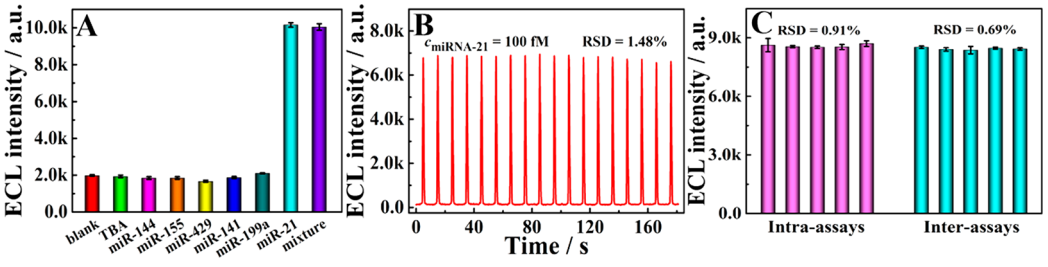

Figure 5. (A) Selectivity of the ECL sensor with different interferences. (B) Stability of the proposed biosensor. (C) Reproducibility of the proposed biosensor.

https://doi.org/10.1021/acsami.1c13086
ACS Appl. Mater. Interfaces 2021, 13, 44079−44085

H_4PTC, the ECL efficiency of Zn-PTC, H_4PTC monomers and H_4PTC aggregates, electrochemical characterization of the ECL biosensor, optimization of the experimental conditions, detection limit calculation, and UV−vis absorption spectroscopy of Zn-PTC (PDF)

AUTHOR INFORMATION

Corresponding Author

Dong-Rong Xiao − *Key Laboratory of Luminescence Analysis and Molecular Sensing (Southwest University), Ministry of Education, College of Chemistry and Chemical Engineering, Southwest University, Chongqing 400715, P.R. China;* orcid.org/0000-0003-4610-1969; Phone: +86-23-68252360; Email: xiaodr98@swu.edu.cn; Fax: +86-23-68254000

Authors

Jun-Mao Wang − *Key Laboratory of Luminescence Analysis and Molecular Sensing (Southwest University), Ministry of Education, College of Chemistry and Chemical Engineering, Southwest University, Chongqing 400715, P.R. China*

Li-Ying Yao − *Key Laboratory of Luminescence Analysis and Molecular Sensing (Southwest University), Ministry of Education, College of Chemistry and Chemical Engineering, Southwest University, Chongqing 400715, P.R. China*

Wei Huang − *Key Laboratory of Luminescence Analysis and Molecular Sensing (Southwest University), Ministry of Education, College of Chemistry and Chemical Engineering, Southwest University, Chongqing 400715, P.R. China*

Yang Yang − *Key Laboratory of Luminescence Analysis and Molecular Sensing (Southwest University), Ministry of Education, College of Chemistry and Chemical Engineering, Southwest University, Chongqing 400715, P.R. China*

Wen-Bin Liang − *Key Laboratory of Luminescence Analysis and Molecular Sensing (Southwest University), Ministry of Education, College of Chemistry and Chemical Engineering, Southwest University, Chongqing 400715, P.R. China;* orcid.org/0000-0002-9086-4974

Ruo Yuan − *Key Laboratory of Luminescence Analysis and Molecular Sensing (Southwest University), Ministry of Education, College of Chemistry and Chemical Engineering, Southwest University, Chongqing 400715, P.R. China;* orcid.org/0000-0003-3664-6236

Complete contact information is available at: https://pubs.acs.org/10.1021/acsami.1c13086

Notes

The authors declare no competing financial interest.

ACKNOWLEDGMENTS

NSFC (21571149) and Chongqing Overseas Returnees Innovation Program (cx2017007 and cx2018026) are acknowledged for supporting this work.

REFERENCES

(1) Chen, K.; Huang, Q.; Fu, T.; Ke, G.; Zhao, Z.; Zhang, X.; Tan, W. MicroRNA-Initiated and Intracellular Na^+-Fueled DNAzyme Motor for Differentiating Molecular Subtypes of Nonsmall Cell Lung Cancer. *Anal. Chem.* **2020**, *92*, 7404−7408.

(2) Jansson, M. D.; Lund, A. H. MicroRNA and Cancer. *Mol. Oncol.* **2012**, *6*, 590−610.

(3) Huang, C.-H.; Huang, T.-T.; Chiang, C.-H.; Huang, W.-T.; Lin, Y.-T. A Chemiresistive Biosensor Based on a Layered Graphene Oxide/Graphene Composite for the Sensitive and Selective Detection of Circulating MiRNA-21. *Biosens. Bioelectron.* **2020**, *164*, 112320.

(4) Wen, Y.; Li, L.; Li, J.; Lin, M.; Liu, G.; Liang, W.; Xu, L.; Li, Y.; Zuo, X.; Ren, S.; Zhu, Y. DNA Framework-Mediated Electrochemical Biosensing Platform for Amplification-Free MicroRNA Analysis. *Anal. Chem.* **2020**, *92*, 4498−4503.

(5) Liu, X.; Wang, X.; Ye, S.; Li, R.; Li, H. A One−Two−Three Multifunctional System for Enhanced Imaging and Detection of Intracellular MicroRNA and Chemogene Therapy. *ACS Appl. Mater. Interfaces* **2021**, *13*, 27825−27835.

(6) Xing, Y.; Cai, Z.; Xu, M.; Ju, W.; Luo, X.; Hu, Y.; Liu, X.; Kang, T.; Wu, P.; Cai, C.; Zhu, J.-J. Raman Observation of a Molecular Signaling Pathway of Apoptotic Cells Induced by Photothermal Therapy. *Chem. Sci.* **2019**, *10*, 10900−10910.

(7) Liu, J.-L.; Tang, Z.-L.; Zhuo, Y.; Chai, Y.-Q.; Yuan, R. Ternary Electrochemiluminescence System Based on Rubrene Microrods as Luminophore and Pt Nanomaterials as Coreaction Accelerator for Ultrasensitive Detection of MicroRNA from Cancer Cells. *Anal. Chem.* **2017**, *89*, 9108−9115.

(8) Qi, H.; Zhang, C. Electrogenerated Chemiluminescence Biosensing. *Anal. Chem.* **2020**, *92*, 524−534.

(9) Chen, Y.; Zhou, S.; Li, L.; Zhu, J.-J. Nanomaterials-Based Sensitive Electrochemiluminescence Biosensing. *Nano Today* **2017**, *12*, 98−115.

(10) Wang, H.-J.; He, Y.; Chai, Y.-Q.; Yuan, R. A Super Intramolecular Self-Enhanced Electrochemiluminescence Immunosensor Based on Polymer Chains Grafted on Palladium Nanocages. *Nanoscale* **2014**, *6*, 10316−10322.

(11) Liu, Z.; Qi, W.; Xu, G. Recent Advances in Electrochemiluminescence. *Chem. Soc. Rev.* **2015**, *44*, 3117−3142.

(12) Ito, H.; Segawa, Y.; Murakami, K.; Itami, K. Polycyclic Arene Synthesis by Annulative π-Extension. *J. Am. Chem. Soc.* **2019**, *141*, 3−10.

(13) Liu, J.-L.; Tang, Z.-L.; Zhang, J.-Q.; Chai, Y.-Q.; Zhuo, Y.; Yuan, R. Morphology-Controlled 9,10-Diphenylanthracene Nanoblocks as Electrochemiluminescence Emitters for MicroRNA Detection with One-Step DNA Walker Amplification. *Anal. Chem.* **2018**, *90*, 5298−5305.

(14) Huang, Y.; Xing, J.; Gong, Q.; Chen, L.-C.; Liu, G.; Yao, C.; Wang, Z.; Zhang, H.-L.; Chen, Z.; Zhang, Q. Reducing Aggregation Caused Quenching Effect through Co-Assembly of PAH Chromophores and Molecular Barriers. *Nat. Commun.* **2019**, *10*, 169.

(15) Hong, Y.; Lam, J. W. Y.; Tang, B. Z. Aggregation-Induced Emission. *Chem. Soc. Rev.* **2011**, *40*, 5361−5388.

(16) Shih, P. I.; Chuang, C. Y.; Chien, C. H.; Diau, E. W. G.; Shu, C. F. Highly Efficient Non-Doped Blue-Light-Emitting Diodes Based on an Anthrancene Derivative End-Capped with Tetraphenylethylene Groups. *Adv. Funct. Mater.* **2007**, *17*, 3141−3146.

(17) Huang, J.; Su, J.-H.; Tian, H. The Development of Anthracene Derivatives for Organic Light-Emitting Diodes. *J. Mater. Chem.* **2012**, *22*, 10977−10989.

(18) Zhao, Z.; Lu, P.; Lam, J. W. Y.; Wang, Z.; Chan, C. Y. K.; Sung, H. H. Y.; Williams, I. D.; Ma, Y.; Tang, B. Z. Molecular Anchors in the Solid State: Restriction of Intramolecular Rotation Boosts Emission Efficiency of Luminogen Aggregates to Unity. *Chem. Sci.* **2011**, *2*, 672−675.

(19) Winnik, F. M. Photophysics of Preassociated Pyrenes in Aqueous Polymer Solutions and in Other Organized Media. *Chem. Rev.* **1993**, *93*, 587−614.

(20) Zhao, Z.; Chen, S.; Lam, J. W. Y.; Lu, P.; Zhong, Y.; Wong, K. S.; Kwok, H. S.; Tang, B. Z. Creation of Highly Efficient Solid Emitter by Decorating Pyrene Core with AIE-Active Tetraphenylethene Peripheries. *Chem. Commun.* **2010**, *46*, 2221−2223.

(21) Zhao, Q.; Zhang, S.; Liu, Y.; Mei, J.; Chen, S.; Lu, P.; Qin, A.; Ma, Y.; Sun, J. Z.; Tang, B. Z. Tetraphenylethenyl-Modified Perylene Bisimide: Aggregation-Induced Red Emission, Electrochemical Properties and Ordered Microstructures. *J. Mater. Chem.* **2012**, *22*, 7387−7394.

(22) Zhao, Q.; Zhang, X. A.; Wei, Q.; Wang, J.; Shen, X. Y.; Qin, A.; Sun, J. Z.; Tang, B. Z. Tetraphenylethene Modified Perylene Bisimide: Effect of the Number of Substituents on AIE Performance. *Chem. Commun.* **2012**, *48*, 11671−11673.
(23) Huang, W.; Hu, G.-B.; Yao, L.-Y.; Yang, Y.; Liang, W.-B.; Yuan, R.; Xiao, D.-R. Matrix Coordination-Induced Electrochemiluminescence Enhancement of Tetraphenylethylene-Based Hafnium Metal−Organic Framework: An Electrochemiluminescence Chromophore for Ultrasensitive Electrochemiluminescence Sensor Construction. *Anal. Chem.* **2020**, *92*, 3380−3387.
(24) Yang, Y.; Hu, G.-B.; Liang, W.-B.; Yao, L.-Y.; Huang, W.; Zhang, Y.-J.; Zhang, J.-L.; Wang, J.-M.; Yuan, R.; Xiao, D.-R. An AIEgen-Based 2D Ultrathin Metal−Organic Layer as an Electrochemiluminescence Platform for Ultrasensitive Biosensing of Carcinoembryonic Antigen. *Nanoscale* **2020**, *12*, 5932−5941.
(25) Huang, W.; Hu, G.-B.; Liang, W.-B.; Wang, J.-M.; Lu, M.-L.; Yuan, R.; Xiao, D.-R. Ruthenium(II) Complex-Grafted Hollow Hierarchical Metal−Organic Frameworks with Superior Electrochemiluminescence Performance for Sensitive Assay of Thrombin. *Anal. Chem.* **2021**, *93*, 6239−6245.
(26) Yang, Y.; Hu, G.-B.; Liang, W.-B.; Yao, L.-Y.; Huang, W.; Yuan, R.; Xiao, D.-R. A Highly Sensitive Self-Enhanced Aptasensor Based on a Stable Ultrathin 2D Metal−Organic Layer with Outstanding Electrochemiluminescence Property. *Nanoscale* **2019**, *11*, 10056−10063.
(27) Yao, L.-Y.; Yang, F.; Hu, G.-B.; Yang, Y.; Huang, W.; Liang, W.-B.; Yuan, R.; Xiao, D.-R. Restriction of Intramolecular Motions (RIM) by Metal-Organic Frameworks for Electrochemiluminescence Enhancement: 2D Zr12-adb Nanoplate as a Novel ECL Tag for the Construction of Biosensing Platform. *Biosens. Bioelectron.* **2020**, *155*, 112099.
(28) Liu, Y.; Zhao, X.; Fang, C.; Ye, Z.; He, Y.-B.; Lei, D.; Yang, J.; Zhang, Y.; Li, Y.; Liu, Q.; Huang, Y.; Zeng, R.; Kang, L.; Liu, J.; Huang, Y.-H. Activating Aromatic Rings as Na-Ion Storage Sites to Achieve High Capacity. *Chem.* **2018**, *4*, 2463−2478.
(29) Zhao, J.; Li, M.; Sun, J.; Liu, L.; Su, P.; Yang, Q.; Li, C. Metal-Oxide Nanoparticles with Desired Morphology Inherited from Coordination-Polymer Precursors. *Chem. - Eur. J.* **2012**, *18*, 3163−3168.
(30) Bai, W.; Cui, A.; Liu, M.; Qiao, X.; Li, Y.; Wang, T. Signal-Off Electrogenerated Chemiluminescence Biosensing Platform Based on the Quenching Effect between Ferrocene and $Ru(bpy)_3^{2+}$-Functionalized Metal−Organic Frameworks for the Detection of Methylated RNA. *Anal. Chem.* **2019**, *91*, 11840−11847.
(31) Hu, G.-B.; Xiong, C.-Y.; Liang, W.-B.; Zeng, X.-S.; Xu, H.-L.; Yang, Y.; Yao, L.-Y.; Yuan, R.; Xiao, D.-R. Highly Stable Mesoporous Luminescence-Functionalized MOF with Excellent Electrochemiluminescence Property for Ultrasensitive Immunosensor Construction. *ACS Appl. Mater. Interfaces* **2018**, *10*, 15913−15919.
(32) Hu, G.-B.; Xiong, C.-Y.; Liang, W.-B.; Yang, Y.; Yao, L.-Y.; Huang, W.; Luo, W.; Yuan, R.; Xiao, D.-R. Highly Stable Ru-Complex-Grafted 2D Metal-Organic Layer with Superior Electrochemiluminescent Efficiency as a Sensing Platform for Simple and Ultrasensitive Detection of Mucin 1. *Biosens. Bioelectron.* **2019**, *135*, 95−101.
(33) Yao, L.-Y.; Yang, F.; Liang, W.-B.; Hu, G.-B.; Yang, Y.; Huang, W.; Yuan, R.; Xiao, D.-R. Ruthenium Complex Doped Metal-Organic Nanoplate with High Electrochemiluminescent Intensity and Stability for Ultrasensitive Assay of Mucin 1. *Sens. Actuators, B* **2019**, *292*, 105−110.
(34) Yang, Y.; Hu, G.-B.; Liang, W.-B.; Yao, L.-Y.; Huang, W.; Yuan, R.; Xiao, D.-R. A Highly Eensitive Self-Enhanced Aptasensor Based on a Stable Ultrathin 2D Metal−Organic Layer with Outstanding Electrochemiluminescence Property. *Nanoscale* **2019**, *11*, 10056−10063.
(35) Kaiser, T. E.; Wang, H.; Stepanenko, V.; Würthner, F. Supramolecular Construction of Fluorescent J-Aggregates Based on Hydrogen-Bonded Perylene Dyes. *Angew. Chem., Int. Ed.* **2007**, *46*, 5541−5544.
(36) Würthner, F.; Kaiser, T. E.; Saha-Möller, C. R. J-Aggregates: From Serendipitous Discovery to Supramolecular Engineering of Functional Dye Materials. *Angew. Chem., Int. Ed.* **2011**, *50*, 3376−3410.
(37) Sun, P.; Wu, Q.; Sun, X.; Miao, H.; Deng, W.; Zhang, W.; Fan, Q.; Huang, W. J-Aggregate Squaraine Nanoparticles with Bright NIR-II Fluorescence for Imaging Guided Photothermal Therapy. *Chem. Commun.* **2018**, *54*, 13395−13398.
(38) Peng, X.; Wen, Z.-B.; Yang, P.; Chai, Y.-Q.; Liang, W.-B.; Yuan, R. Biomimetic 3D DNA Nanomachine via Free DNA Walker Movement on Lipid Bilayers Supported by Hard SiO_2@CdTe Nanoparticles for Ultrasensitive MicroRNA Detection. *Anal. Chem.* **2019**, *91*, 14920−14926.
(39) Rashidnadimi, S.; Hung, T. H.; Wong, K.-T.; Bard, A. J. Electrochemistry and Electrogenerated Chemiluminescence of 3,6-Di(spirobifluorene)-*N*-phenylcarbazole. *J. Am. Chem. Soc.* **2008**, *130*, 634−639.
(40) Swanick, K. N.; Sandroni, M.; Ding, Z.; Zysman-Colman, E. Enhanced Electrochemiluminescence from a Stoichiometric Ruthenium(II)−Iridium(III) Complex Soft Salt. *Chem. - Eur. J.* **2015**, *21*, 7435−7440.
(41) Dixit, C. K.; Vashist, S. K.; O'Neill, F. T.; O'Reilly, B.; MacCraith, B. D.; O'Kennedy, R. Development of a High Sensitivity Rapid Sandwich ELISA Procedure and its Comparison with the Conventional Approach. *Anal. Chem.* **2010**, *82*, 7049−7052.
(42) Lu, J.; Wang, J.; Hu, X.; Gyimah, E.; Yakubu, S.; Wang, K.; Wu, X.; Zhang, Z. Electrochemical Biosensor Based on Tetrahedral DNA Nanostructures and G-Quadruplex−Hemin Conformation for the Ultrasensitive Detection of MicroRNA-21 in Serum. *Anal. Chem.* **2019**, *91*, 7353−7359.
(43) Zhu, D.; Wei, Y.; Sun, T.; Zhang, C.; Ang, L.; Su, S.; Mao, X.; Li, Q.; Fan, C.; Zuo, X.; Chao, J.; Wang, L. Encoding DNA Frameworks for Amplified Multiplexed Imaging of Intracellular MicroRNAs. *Anal. Chem.* **2021**, *93*, 2226−2234.
(44) Xu, Z.-H.; Gao, H.; Zhang, N.; Zhao, W.; Cheng, Y.-X.; Xu, J.-J.; Chen, H.-Y. Ultrasensitive Nucleic Acid Assay Based on Cyclometalated Iridium(III) Complex with High Electrochemiluminescence Efficiency. *Anal. Chem.* **2021**, *93*, 1686−1692.
(45) Zhao, M.-L.; Zeng, W.-J.; Chai, Y.-Q.; Yuan, R.; Zhuo, Y. An Affinity-Enhanced DNA Intercalator with Intense ECL Embedded in DNA Hydrogel for Biosensing Applications. *Anal. Chem.* **2020**, *92*, 11044−11052.
(46) Ying, Z.-M.; Wu, Z.; Tu, B.; Tan, W.; Jiang, J.-H. Genetically Encoded Fluorescent RNA Sensor for Ratiometric Imaging of MicroRNA in Living Tumor Cells. *J. Am. Chem. Soc.* **2017**, *139*, 9779−9782.

https://doi.org/10.1021/acsami.1c13086
ACS Appl. Mater. Interfaces 2021, 13, 44079−44085